

Quantum reflection of a Bose-Einstein condensate with a dark soliton from a step potential

Dong-Mei Wang(王冬梅), Jian-Chong Xing(邢健崇), Rong Du(杜荣), Bo Xiong(熊波), and Tao Yang(杨涛)
Citation: Chin. Phys. B, 2021, 30 (**12**): 120303. DOI: 10.1088/1674-1056/ac051e
Journal homepage: http://cpb.iphy.ac.cn; http://iopscience.iop.org/cpb

What follows is a list of articles you may be interested in

Quantum reflection of a Bose-Einstein condensate with a dark soliton from a step potential

Dong-Mei Wang(王冬梅), Jian-Chong Xing(邢健崇), Rong Du(杜荣), Bo Xiong(熊波), and Tao Yang(杨涛)
Chin. Phys. B, 2021, 30 (**12**): 120303. DOI: 10.1088/1674-1056/ac051e

Adjustable half-skyrmion chains induced by SU(3) spin-orbit coupling in rotating Bose-Einstein condensates

Li Wang(王力), Ji Li(李吉), Xiao-Lin Zhou(周晓林), Xiang-Rong Chen(陈向荣), and Wu-Ming Liu(刘伍明)
Chin. Phys. B, 2021, 30 (**11**): 110312. DOI: 10.1088/1674-1056/abfcc8

Dynamics of bright soliton in a spin-orbit coupled spin-1 Bose-Einstein condensate

Hui Guo(郭慧), Xu Qiu(邱旭), Yan Ma(马燕), Hai-Feng Jiang(姜海峰), and Xiao-Fei Zhang(张晓斐)
Chin. Phys. B, 2021, 30 (**6**): 060310. DOI: 10.1088/1674-1056/abf34a

Dynamical stability of dipolar condensate in a parametrically modulated one-dimensional optical lattice

Ji-Li Ma(马吉利), Xiao-Xun Li(李晓旬), Rui-Jin Cheng(程瑞锦), Ai-Xia Zhang(张爱霞), and Ju-Kui Xue(薛具奎)
Chin. Phys. B, 2021, 30 (**6**): 060307. DOI: 10.1088/1674-1056/abd746

Spin-orbit-coupled spin-1 Bose-Einstein condensates confined in radially periodic potential

Ji Li(李吉), Tianchen He(何天琛), Jing Bai(白晶), Bin Liu(刘斌), and Huan-Yu Wang(王寰宇)
Chin. Phys. B, 2021, 30 (**3**): 030302. DOI: 10.1088/1674-1056/abc53e

---

Quantum reflection of a Bose–Einstein condensate with a dark soliton from a step potential*

Dong-Mei Wang(王冬梅)[1], Jian-Chong Xing(邢健崇)[1], Rong Du(杜荣)[1], Bo Xiong(熊波)[2,†], and Tao Yang(杨涛)[1,3,4,‡]

[1] *Shaanxi Key Laboratory for Theoretical Physics Frontiers, Institute of Modern Physics, Northwest University, Xi'an* 710127, *China*
[2] *School of Science, Wuhan University of Technology, Wuhan* 430070, *China*
[3] *School of Physics, Northwest University, Xi'an* 710127, *China*
[4] *Peng Huanwu Center for Fundamental Theory, Xi'an* 710127, *China*

(Received 28 March 2021; revised manuscript received 19 April 2021; accepted manuscript online 26 May 2021)

We study dynamical behaviors of a Bose–Einstein condensate (BEC) containing a dark soliton reflected from potential wells and potential barriers, respectively. The orientation angle of the dark soliton and the width of the potential change play key roles on the reflection probability R_s. Variation of the reflection probability with respect to the orientation angle θ of the dark soliton can be well described by a cosine function $R_s \sim \cos[\lambda(\theta - \pi/2)]$, where λ is a parameter determined by the width of the potential change. There are two characteristic lengths which determine the reflection properties. The dependence of the reflection probability on the width of the potential change shows distinct characters for potential wells and potential barriers. The length of the dark soliton determines the sensitive width of potential wells, whereas for potential barriers, the decay length of the matter wave in the region of the barrier qualifies the sensitive width of the barrier. The time evolution of the density profiles of the system during the reflection process is studied to disclose the different behaviors of matter waves in the region of the potential variation.

Keywords: Bose–Einstein condensate, dark soliton, quantum reflection

PACS: 03.75.Nt, 05.45.Yv, 34.50.–s **DOI:** 10.1088/1674-1056/ac051e

1. Introduction

Quantum reflection is a classically counterintuitive phenomenon whereby particles are reflected from potential barriers or wells without reaching a classical turning point.[1,2] Such a phenomenon has been observed in various systems, such as atomic mirror,[3–5] nanoporous media,[6,7] rough surfaces,[8] and Si, BK7 glass surface.[9] Recent developments are extended to cold atomic systems in which quantum reflections of ultra-cold atoms appear on the potential of solid surfaces[10,11] as well as on the various structures, such as graphene,[12] semiconductor superstructures and thin films.[13] Since significant reflection occurs under the condition $\phi(k) = (1/k^2)\mathrm{d}k/\mathrm{d}x_s \sim \mathrm{d}\lambda/\mathrm{d}x_s \gg 1$,[9] where the local wave number, $k = 2\pi/\lambda$, depends on the de Broglie wave length λ, and x_s is the normal distance from the atom to the surface, the system of ultracold and quantum degenerate atomic gases with large de Broglie wave lengths is an excellent platform for experiments to study quantum reflection at normal incidence with large flexibility on the control of the atomic motion.

Solitons are self-reinforcing wavepackets, which maintain their shapes when propagating over long distances, and emerge from collisions unaltered.[14,15] The existence of such localized wavepackets indicates nontrivial effects from nonlinear interactions, and they have been observed in different systems, including water waves,[16] plasmas,[17,18] and nonlinear optics.[19,20] Theoretically, solitons in nonlinear media were described numerically[21] and analytically[22] half a century ago, and have been confirmed in different fields such as oceanography, biology, and fiber optics. Afterwards, the atomic solitons were also investigated in various platforms, such as optical systems,[23] magnetic films,[24] and waveguide arrays.[25] Recently, solitons in ultracold atomic systems, e.g., Bose–Einstein condensates, have attracted much attention. Especially, such solitons can theoretically be interpreted well by the well-known Gross–Pitaevskii (GP) equation.[26,27] Experimentally, a matter-wave dark soliton with a phase difference of π can be generated readily by appropriate phase imprinting,[28,29] density engineering,[30] sweeping a dipole potential through the condensate,[31,32] as a consequence of quantum shock, and from the local minima of interference fringes.[33,34]

In recent years, a great deal of experimental and theoretical work has been involved with the quantum reflection of condensates. Conventionally, the incident velocity of the condensate has a significant effect on the reflection process, and when

*Project supported by the National Natural Science Foundation of China (Grant Nos. 11775178, 12075175, 11934015, and 12047502), the Major Basic Research Program of Natural Science of Shaanxi Province, China (Grant Nos. 2017KCT-12 and 2017ZDJC-32), and the Open Research Fund of Shaanxi Key Laboratory for Theoretical Physics Frontiers (Grant No. SXKLTPF-K20190602).

†Corresponding author. E-mail: boxiongpd@gmail.com
‡Corresponding author. E-mail: yangt@nwu.edu.cn

© 2021 Chinese Physical Society and IOP Publishing Ltd

the velocity of the condensate is low, an abnormal reflectivity has been observed experimentally.[6,11] The probable explanation attributes it to interatomic interactions, which may lead to nonlinear excitations that slow down the center-of-mass motion of the matter wave and result in disruptions.[10,35,36] Due to the surprising robustness of bright matter-wave solitons, its collision and associated regions of chaotic dynamics have been addressed.[37,38] Also, the quantum reflection of such bright solitons has been discussed intensively.[15,39] Moreover, the dynamics of moving bright solitons in a polarized BEC with spin-orbit coupling has been studied, showing that the speed of a soliton dominates its structure.[40] Both stationary bright solitons and moving bright solitons can be found in a spin-orbit-coupled condensate.[41] In contrast to bright solitons, reflection of a dark matter-wave soliton has not yet been well investigated, particularly in its structure. Some theoretical works have addressed the role of the nonlinear excitations, such as dark solitons and vortices, in the quantum reflection of the condensate interacting with a solid surface or a gaussian potential.[42–44] For matter-wave dark solitons in boxlike traps, dissipative reflections occur with soft boundaries.[45] A recent work also shows that the orientation of a two-dimensional (2D) dark soliton can significantly affect the reflection probability of the condensate from a sharp potential barrier due to the rotational symmetry broken.[44] However, the essential factors for such influence have not been clarified. Moreover, influence of a 2D dark soliton, especially its configuration, on the quantum reflection subject to a potential well has not yet been investigated. Correspondingly, differences between the reflections of a BEC with a dark soliton from a potential well and a potential barrier are still unclear. In this paper, we investigate the dynamical behavior of a 2D disk-shaped Bose–Einstein condensate containing a dark soliton separately reflected from square potential wells and potential barriers. We try to find the influence of the orientation angle of a dark soliton, the structure of the potential and the width of the potential variation on the quantum reflection probability. We further use dynamical images of the density profiles of the condensates to reflect the physical mechanism through numerical simulations. The underlying mechanism of the quantum reflection is discussed intensively.

2. Method and simulation scheme

We consider a ^{23}Na BEC containing N atoms, which are initially trapped by a harmonic trapping potential of the form $V_{\rm h}(x,y,z) = m(\omega_x^2x^2+\omega_y^2y^2+\omega_z^2z^2)/2$. Here we choose the trap frequencies to be $\omega = \omega_x = \omega_y = 2\pi\times 10$ Hz and $\omega_z = 2\pi\times 100$ Hz so that the trap frequency in the z direction is much larger than those in the x and y directions. One can verify that the chemical potential in the radial directions is much smaller than the confining oscillator energy in the axial direction. Hence, the system can be treated as a disk-shaped 2D condensate. The dynamics of such a system at zero temperature are well described by the 2D time-dependent GP equation

$$\mathrm{i}\hbar\partial_t\psi = -\frac{\hbar^2}{2m}\nabla^2\psi + V(x,y)\psi + gN|\psi|^2\psi, \tag{1}$$

where $\psi(x,y,t)$ is the temporal condensate wave function with $N = 1.8\times10^4$ in our calculations. The 2D coupling constant is $g = 2\sqrt{2\pi}\hbar\omega_z a_{\rm s}a_z$ with the s-wave scattering length $a_{\rm s} = 2.9$ nm. The radial and axial oscillation lengths are $x_0 = \sqrt{\hbar/m\omega}$ and $a_z = \sqrt{\hbar/m\omega_z}$, respectively. The ground state of the dark soliton is obtained by the imaginary time evolution of the GP equation, where a π phase step is added into the condensate wave function so that two stable density halves are formed. We use x_0, $t_0 = 1/\omega$, $E_0 = \hbar\omega$ as the units of length, time and energy, respectively, to derive the dimensionless GP equation for a better accuracy of our simulations.

To get a prevalent insight about the interaction between a dark soliton and a potential energy surface, we consider a general potential which is in combination of a harmonic trap and a potential barrier/well of the form

$$V(x,y) = \begin{cases} V_{\rm h}(x,y), & x<0, \\ V_0, & x\in[0,d], \\ 0, & x>d \end{cases} \tag{2}$$

where $V_0>0$ and $V_0<0$ correspond to the potential barrier and potential well, respectively, and d is the width of the potential barrier or well. We note that in the region of the potential drop, the velocity of the condensate is much larger than the incident velocity, which makes that a sufficiently small grid size is required to avoid the distortion arisen from the finite size scale. In our calculations, we use 4000×1000 grids, and the grid size is $0.01\sqrt{2}x_0$ to make the results of our calculations reliable.

We consider two different potential profiles: potential I [Fig. 1(a)] is a potential barrier of width d; potential II [Fig. 1(b)] is a potential well of width d. The abrupt change of the potentials chosen here fulfills readily the quantum reflection condition and makes the reflection of solitons prominent. Thus it enables us to identify the key physical processes occurring when the BEC experiences reflection, and to sharpen the understanding needed for experimental studies to explain BECs with solitons reflected from more complex semiconductor surface potentials or nanostructure potentials. The center of mass of the condensate is initially placed at the position $(\Delta_x,0)$ away from the center of the harmonic trap. In this research, we always consider the normal incident of condensates towards the energy potential surface. Due to the variation of the trap potential, the condensate cloud is driven to move towards the potential barrier or the potential well, which allows us to study the reflection process of the condensate containing a dark soliton. Figures 1(c) and 1(d) show a typical density distribution and the corresponding phase distribution of

the initial state of a condensate containing a dark soliton with the orientation angle $\theta = \pi/4$, respectively. When the solitons are initially imprinted in the condensate, we can freely adjust the angle between the dark solitons and the positive x-axis.

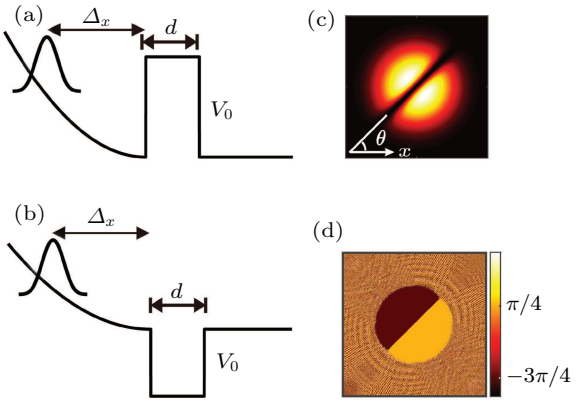


Fig. 1. A schematic view of the systems. A condensate cloud containing a dark soliton interacting with a potential barrier (a) and a potential well (b) for the initial center-of-mass displacement in the x direction being Δ_x. (c) and (d) The top view of the initial density distribution and the corresponding phase distribution of a condensate with the orientation angle of the dark soliton being $\theta = \pi/4$.

A condensate carrying a dark soliton has two specific length scales determined by the interatomic interaction, the Thomas–Fermi (TF) radius $R_{\rm TF} = (4g/\pi m\omega^2)^{1/4}$ characterizing the size of the condensate cloud and the healing length $\xi = \hbar/\sqrt{2ngm} \simeq 0.5x_0$ correlated to the width of the soliton with n being the density of the condensate. For the parameters used in our calculations, we have $R_{\rm TF} = 3.58x_0$ for a bare condensate without a dark soliton. The half width of the condensate with a dark soliton is about $5.67x_0$. For a potential well, the typical width is such that the soliton structure can be completely maintained in the well, i.e., $d = 11x_0 \approx 75$ μm for the parameters used in our simulations. For a potential barrier, the typical width is the decay length which is determined by the decay rate of the wave function of the condensate within the barrier region. Current cold-atom experiments can achieve box-like potentials with length varying from several micrometers to hundreds of micrometers,[46,47] so the potential wells we considered can be realized experimentally. A relatively large interatomic interaction leads to a small healing length, resulting in formation of a large size of ground-state BEC with a small width of the dark soliton. Note that such an interatomic interaction will not change essentially our conclusion here if many excitations are not involved in the process of reflection. The size of the condensate can be adjusted by changing the trap frequencies or the interatomic interactions experimentally.

To explore the role of a dark soliton in the quantum reflection of a BEC from potential energy surfaces, it is required that the lifetime of the dark soliton should be larger than the timescale of the reflection process. Since the dark soliton in 2D BECs is generally unstable, it will eventually decay into vortices due to the snake instability. This indicates that the complete quantum reflection should appear before the distortion of the dark soliton. Previous work showed that for some specific parameters the lifetime of the dark soliton either located in the middle of a 2D condensate is larger than the timescale of the reflection process.[44] We also note that the stability of a 2D dark soliton in trapped BECs is still an interesting topic.

3. Results and discussion

As stated in Refs. [48,49], the center-of-mass velocity and interatomic interaction of condensates play important roles in formation of interference patterns and dynamic excitations. These two factors determine time scales of interference of BECs and the distortion of solitons. The dynamics of the system are determined by the competition of these two time scales. As the condensate moves towards the trap center, its average incident velocity at the edge of the potential well or barrier is approximately $\bar{v} \approx \omega\sqrt{\Delta_x^2 + \Delta_y^2}$. Previous research showed that at low incident velocities and high densities, the nonlinear interatomic interactions dominate the reflection process of a BEC from a silicon surface, which results in formation of solitons and vortices and anomalous quantum reflection.[10]

Here, we further study quantum reflection of BECs originally containing a dark soliton from an abrupt change of the potential in space, and specifically concentrate on the role of the initial configuration of the dark soliton and the width of the potential variation in such a reflection process. To demonstrate explicitly our findings, we define the time dependent number of atoms on the left hand side of the step function ($x \in [-L/2, 0]$) in the form of

$$N_l(t) = \frac{1}{N}\int_{-\frac{L}{2}}^{0}\int_{-\frac{L}{2}}^{\frac{L}{2}} |\psi(x,y,t)|^2 \mathrm{d}x\mathrm{d}y, \tag{3}$$

where L is the size of the system in our calculations. We employ $R_{\rm s}$ to denote the reflection probability (asymptotic value of $N_l(t)$) after the condensate cloud has been completely separated from the surface of the potential barrier or well. When the height of the potential barrier or the depth of the potential well, $|V_0|$, is large enough, the condensate cloud undergoes the elastic reflection with $R_{\rm s}$ close to 1, which is similar to its classical counterpart. For systems without interatomic interactions, the reflection probability depends only on the incident velocity (the displacement Δ_x of the condensate in the x direction in our systems). However, for interacting systems, the momenta of the x and y directions can transform mutually during the reflection process, which will in turn affect the dynamics of the system. However, as we only consider the normal incident clouds, there is no initial potential energy in the y direction.

Previous work showed that when a BEC with a dark soliton is reflected from a potential barrier, its asymptotic reflection probability R_s is highly sensitive to the initial orientation angle θ of the soliton.[44] Here we further consider the behavior of such a BEC reflected from a potential well. We find that R_s is still sensitive to θ for potential wells. However, the variation of R_s shows abundant modes with respect to different widths of the potential well. In Fig. 2(a), we show three typical examples of the R_s–θ curves for different d. It is found that the relation between R_s and θ can be written as

$$R_s = R_0 + R_{se}\cos[\lambda(\theta - \pi/2)], \tag{4}$$

with R_0, R_{se} and λ being adjustable parameters. For $d = 4.2x_0$ as denoted by the red solid curve with squares, the fitting parameters are $R_0 = 0.42$, $R_{se} = 0.04$ and $\lambda = 2.25$, respectively. For $d = 4.7x_0$, the fitting parameters are $R_0 = 0.38$, $R_{se} = -0.12$ and $\lambda = 1.61$, respectively. This case is similar to the R_s–θ curve of the reflection from a potential barrier as shown in Fig. 2(b), which can be well fitted by employing $\lambda = 2$ with $\Delta_x = 7.05x_0$, $R_0 = 0.935$ and $R_{se} = 0.045$. For $d = 12.7x_0$, R_s nearly does not change with θ as denoted by the purple solid line with diamonds in Fig. 2(a). We note that for both potential wells and potential barriers, $\theta = \pi/2$, i.e., the dark soliton parallel to the surface where the reflection occurs is a special configuration. For potential barriers, R_s always takes the minimum for any value of d at $\theta = \pi/2$, while for potential wells, R_s may take the minimum or maximum according to different values of d. In Fig. 2(c), we give typical density distributions of the condensate with a $\theta = \pi/4$ dark soliton (see Fig. 1(c)) during the reflection. For a potential well, the orientations of the dark soliton in the confined part within the potential well (α_1) and in the transmitted part of the condensate (α_2) with respect to the orientation of the reflected dark soliton may be different from that of the incident cloud (2θ). However, for a potential barrier, the orientations of the dark soliton in the transmitted cloud and the incident cloud are always 2θ. We note that for potential wells, R_{se} can be positive and negative, while it is always positive for potential barriers.

In Fig. 3, we show the influence of the width of the step potentials in the quantum reflection probability of the condensate cloud containing a dark soliton. We find that when the width of the potential well is less than the length of the soliton (or the condensate), i.e., $d < 11.34x_0$, the reflection probability R_s is sensitive to d as well as the initial orientation of the dark soliton θ. For different initial orientations, R_s displays a regular oscillation with an envelope of exponential decay towards a stable value, $R_s \simeq 0.37$, when d is larger than $11.34x_0$ as shown in Fig. 3(a). It indicates that the reflection probability is immune against the dark soliton configuration when the width of the potential well is larger than the size of the condensate cloud. We note that for a condensate cloud without a dark soliton, the damped oscillation of the reflection probability with respect to increasing width of the potential well has nearly the same period as that of the case with a $\theta = 0$ dark soliton (red line with circles in Fig. 3(a)) except for a larger amplitude.

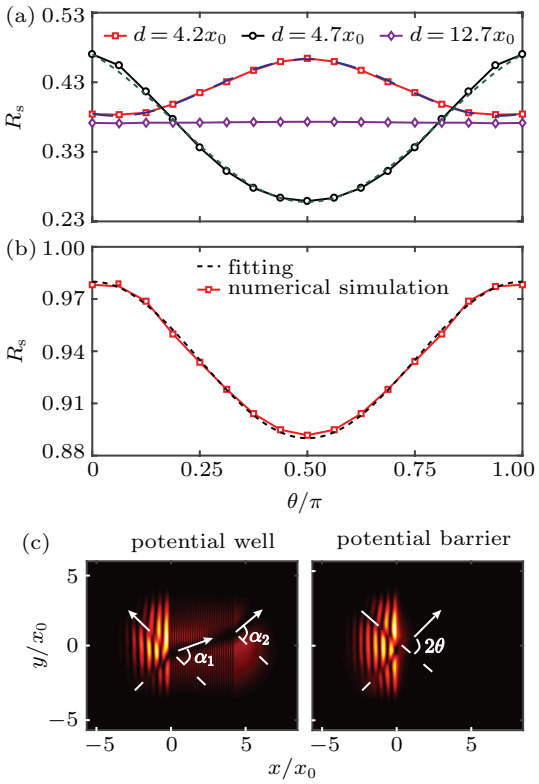


Fig. 2. The reflection probabilities as a function the orientation angle of the dark soliton and the typical Density profiles of the system during the reflection process. (a) The curves of the asymptotic reflection probability (R_s) of a condensate reflected from the potential well with respect to the orientation angle of the dark soliton θ. The red solid line with squares, the black solid line with circles and the purple solid line with diamonds are for the width of the potential well being $d = 4.2x_0$, $d = 4.7x_0$, $d = 12.7x_0$, respectively. The blue dashed line and the green dotted line are the corresponding fitting curves calculated by Eq. (4), respectively. (b) The red solid line with squares is the $R_s(\theta)$ curve of a condensate reflected from the potential barrier with $d = 5.64x_0$, and the black dotted line is the corresponding fitting curve calculated by Eq. (4). (c) The density distribution of the condensate reflected from the surface of the potential well with $d = 4.2x_0$ at $t = 1.68t_0$, and from the surface of the potential barrier with $d = 5.66x_0$ at $t = 1.68t_0$. The angles indicated by the white arrows show the directions of the dark solitons in different parts of the condensate cloud. In upper figures, the parameters used for the potential wells are $V_0 = -180E_0$ and $\Delta_x = 7.05x_0$, and those used for the potential barriers are $V_0 = 40E_0$ and $\Delta_x = 7.05x_0$.

For a square potential barrier, since the kinetic energy of the incident condensate is less than the height of the barrier, i.e., $m\omega^2\Delta_x^2/2 \simeq 24E_0$ is less than $V_0 = 40E_0$, quantum wisdom indicates that the wave function of the condensate will decay exponentially in the form of $\psi \sim e^{-\beta x}$ within the region of the potential barrier. Here we have the decay constant $\beta \simeq \sqrt{2m(V_0 - E)/\hbar^2} = 5.5/x_0$ for the parameters used in Fig. 3(b). Then we can obtain $|\psi|^2 \sim 1.68 \times 10^{-5}$ as $x = x_0$, which means that the decay of the condensate wave function is mainly within the x_0 length scale, and the reflection probability can reach its asymptotic value for d larger than x_0. If d

is smaller than the decay length, the dynamics of the system are dominated by the decay process, and the effect of soliton structure is strongly depressed. However, for d larger than the decay length, the orientation angle of the dark soliton becomes significant resulting in different asymptotic values. This analysis coincides with our numerical results shown in Fig. 3(b).

To see the influence of the orientation of the dark soliton on the reflection probabilities more clearly, we calculate the quantity $\delta R_{\rm s} = R_{\rm s}(\theta = \pi/2) - R_{\rm s}(\theta = 0)$ for potential wells and potential barriers as shown in Figs. 3(c) and 3(d), respectively. The $\delta R_{\rm s}$–d curve performs a damped oscillation for the potential well (see Fig. 3(c)), which is similar to the $R_{\rm s}$–d curves in Fig. 3(a). This variation can be fitted by the function $\delta R_{\rm s} = -0.74\exp(-0.32d/x_0)\sin(3.42d/x_0 - 9.38)$ (the dotted curve in Fig. 3(c)). For a potential barrier, $\delta R_{\rm s}$ decays exponentially to a nonzero constant with increasing d. It can be fitted well by the function $\delta R_{\rm s} = 0.09\exp(-1.67d/x_0) - 0.09$. Compared to the potential barrier, the reflection from a potential well will be much more sensitive to the orientation of the dark soliton if the width of the potential well is smaller than the size of the condensate, where the amplitude of variation can reach up to 25% with respect to the total reflection. As shown in Fig. 3(d), the reflection from a potential barrier is less sensitive to θ, where the amplitude of variation increases exponentially with d, and is less than 9% with respect to the total reflection.

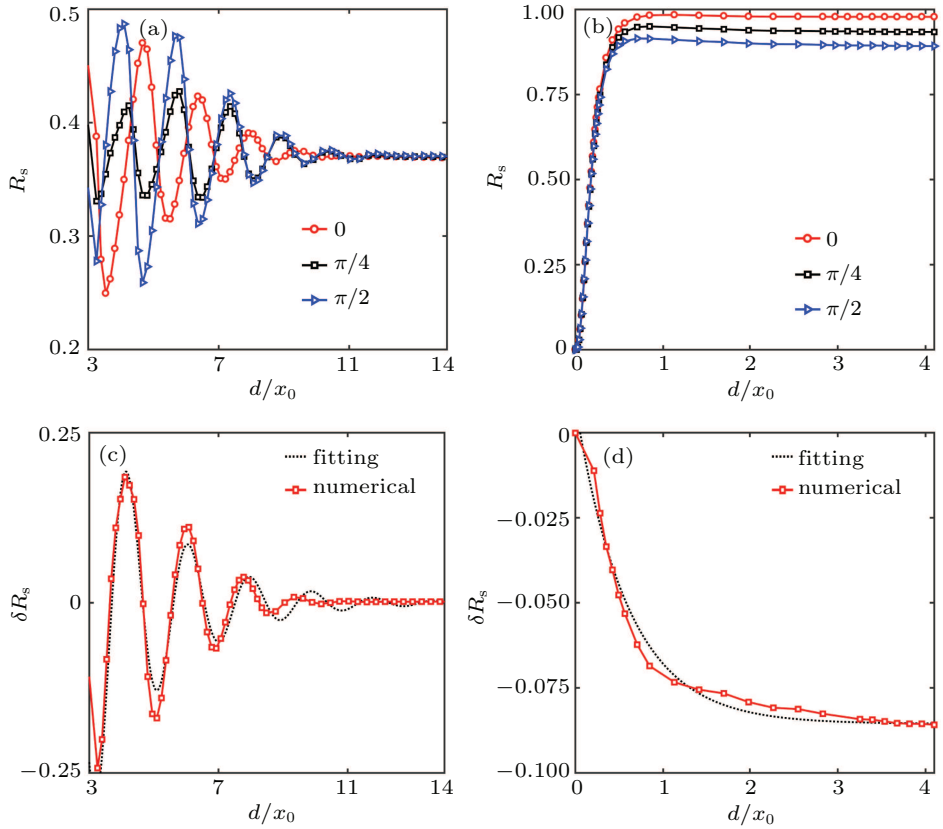


Fig. 3. The reflection probability $R_{\rm s}(\theta)$ and the difference $\delta R_{\rm s}$ between $R_{\rm s}(\pi/2)$ and $R_{\rm s}(0)$ versus the width d of the potential change. (a) The $R_{\rm s}$ curved with respect to d for the orientation angles of the dark solitons are 0 (red solid line with circles), $\pi/4$ (black solid line with squares), and $\pi/2$ (blue solid line with triangles), with $\Delta_x = 7.47x_0$ and $V_0 = -180E_0$. (b) The $R_{\rm s}$ curved with respect to d for the orientation angles of the dark solitons are 0 (red solid line with circles), $\pi/4$ (black solid line with squares), and $\pi/2$ (blue solid line with triangles), with $\Delta_x = 7.05x_0$ and $V_0 = 40E_0$. (c) and (d) The red solid lines with squares are the corresponding $\delta R_{\rm s}$ curves with respect to d of (a) and (b), respectively. The black dotted lines are the corresponding fitting curves.

To explore the reflection behaviors of a condensate containing a dark soliton from a potential well and a potential barrier further, we study the time evolution of the density profile of the condensate cloud. We know that a incident wave with energy E and wave number $\sqrt{2mE/\hbar^2}$ subject to a square potential V_0 leads to the wave number within the region of the square potential being $\sqrt{2m(E-V_0)/\hbar^2}$. In our calculations, we consider potential wells with $V_0 < 0$ and $E - V_0 \gg E$, resulting in the velocity of the transmitted wave being much higher than that of the incident wave. Such high velocity of the transmitted wave accounts for an interference pattern with very small fringe spacings in the region of the potential wells. This is in contrast with the system of potential barriers, where the order parameter decays exponentially. In Fig. 4, we show the time evolution of the density profile of a condensate containing a $\theta = \pi/2$ dark soliton reflected from a potential well. The self-interference pattern of the condensate cloud within the region of potential well during the reflection process can be identified clearly in the areas surrounded by the white rectangles as shown in Figs. 4(Ib) and 4(Ⅱb) (as well as in Figs. 4(d)

and 4(e)). The interference modes in Figs. 4(d) and 4(e) are obviously different. We argue that the different interference modes due to the different widths of the potential wells may responsible for the distinct R_s–θ behaviors as shown in Fig. 2(b). As shown in Figs. 4((Ic) and 4(Ⅱc)), the dark-soliton can penetrate the potential well and maintain its structure very well in the transmitted part of the condensate cloud, indicating the robustness of the dark soliton structure during the reflection from potential wells. The distortion of the dark soliton in the transmitted part of the condensate cloud is lager for $d = 4.2x_0$ (Fig. 4(Ic)) than that for $d = 4.7x_0$ (Fig. 4(Ⅱc)).

For the reflection of BECs from potential barriers as shown in Fig. 5, no self-interference occurs within the barrier region, which is completely different from the cases of potential wells. With increasing d, Fig. 5 shows the reflection process of the condensate with different orientations for the same potential barrier. When the soliton orientation is parallel to the barrier surface (Fig. 5(Ia)), the soliton structure tends to prevent the return of the reflected wave by barriers due to its self-reinforcement and thus reduces the reflection probability. For $\theta = 0$, the reflection of the condensate can be regarded approximately as the reflection of two symmetric small condensates, and the influence of the dark soliton is trivial. The reflection behavior of the condensate with a $\theta = 0$ dark soliton is identical to that of the condensate without a soliton (see Fig. 2 in Ref. [45]). Therefore, when a BEC containing a dark soliton is reflected from a potential barrier, the reflection probability for $\theta = \pi/2$ is smaller than that for $\theta = 0$ (see Fig. 2(c)). Compared to the potential well reflection, the ability of a dark soliton passing through a potential barrier is much weaker. The soliton structure in the transmitted condensate cloud is not obvious or complete as shown in Figs. 4(Ic) and 4(Ⅱc).

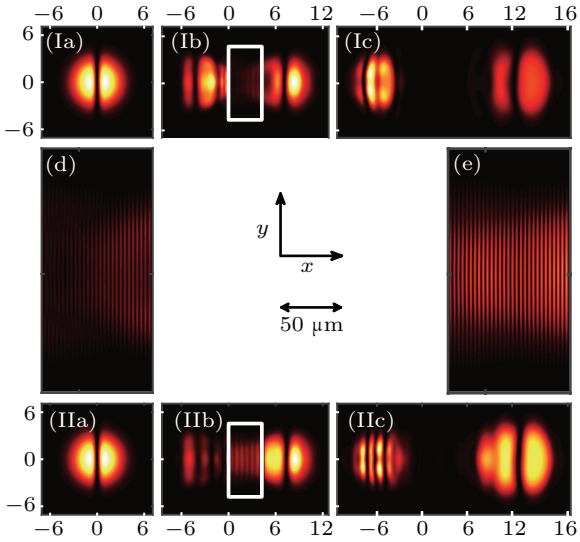


Fig. 4. The typical density profiles of the condensate containing a $\theta = \pi/2$ dark soliton reflected from the potential wells with two different widths. Line I: the reflection for $d = 4.2x_0$. The density distribution of the condensate at $t = 0$ (Ia), $t = 2.16t_0$ (Ib) and $t = 2.88t_0$ (Ic). Line Ⅱ: the reflection for $d = 4.7x_0$, with the corresponding times as the same as those in line I. The depth of the potential well is $V_0 = -180E_0$. (d) and (e) Enlarged figures of region surrounded by the withe rectangles in (Ib) and (Ⅱb), respectively.

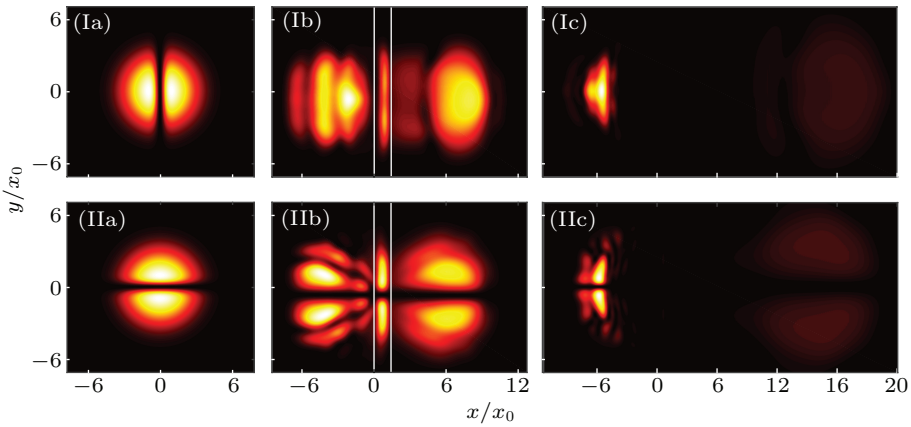


Fig. 5. The typical density profiles of the condensate containing a dark soliton with different orientation angles reflected from a potential barrier. Line I: the density distribution of the condensate containing a dark soliton with $\theta = \pi/2$ at $t = 0$ (Ia), $t = 2.40t_0$ (Ib) and $t = 3.68t_0$ (Ic). Line Ⅱ: the density distribution of the condensate containing a dark soliton with $\theta = 0$, with the corresponding times as the same as those in Line I. The width and the height of the potential barrier are $d = 1.41x_0$ and $V_0 = 20E_0$, respectively.

Moreover, we explore the effects of the expansion motion on the quantum reflection of the system. To clearly isolate the effects, we only consider the potential drop with infinite width. The ground-state BECs are created under different traps: $\omega = 4\omega_0$, $6\omega_0$, and $8\omega_0$. The expansion-dominated motion is triggered by changing the trap frequencies rapidly from their original values to $\omega = \omega_0$ at $t = 0$. Meanwhile, we suddenly displace the harmonic trap by a distance $2.83x_0$. Thus the condensate expands rapidly when it is accelerated towards the potential drop. In Fig. 6, we show the reflection probabilities of the expansion-dominated BECs, R_s, with respect to different orientation angle θ. We can seen clearly that the shapes of the curves are similar to that of the finite potential well with $d = 4.7x_0$ in Fig. 2(b) and that of the barrier potential in Fig. 2(c). Here $\theta = \pi/2$ is still a special configuration with the lowest reflection probability. We find that these

curves can also be well described by Eq. (4). However, the curves are much shallow, and the variations of R_s with respect to θ are only up to 0.05. We note that the significant difference between the systems with expansion and without expansion is that the sensitivity of the reflection probability to the soliton orientation at infinite width of the well. When the expansion is included, R_s is still sensitive to θ at infinite width of the well for the reflections in the potential well systems. This is quite similar to reflections of systems for potential barriers (see Fig. 3(b)). Since the expansion results in the acceleration of center-of-mass of the condensate cloud towards the potential drop, the reflection probability reduces accordingly. As shown in Fig. 6, R_s for larger initial trap frequency is smaller than those for smaller ones, due to the fact that the larger the initial trap frequency is, the higher the expansion speed is.

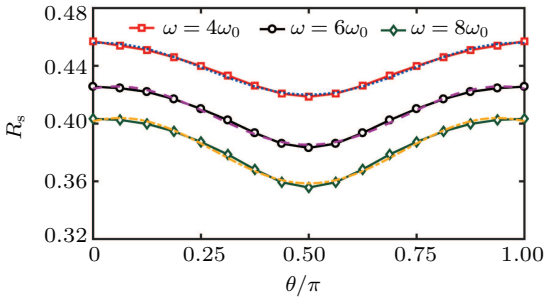


Fig. 6. The reflection probability of the condensates dominated by expansion motions from a infinite wide potential drop as a function of the orientation of the dark soliton. The red solid line with squares, black line with circles and green line with diamonds are for systems with initial trap frequencies $4\omega_0$, $6\omega_0$ and $8\omega_0$, respectively. The depth of the potential well and the initial displacement of the condensate are $V_0 = -180E_0$ and $\Delta_x = 2.83x_0$, respectively. The dotted line ($R_0 = 0.44$, $R_{se} = -0.018$ and $\lambda = 2.07$), dashed line ($R_0 = 0.41$, $R_{se} = -0.020$ and $\lambda = 2.24$) and dash-dotted line ($R_0 = 0.38$, $R_{se} = -0.022$ and $\lambda = 2.28$) are the fitting curves calculated by Eq. (4).

4. Conclusion

In summary, we have investigated some crucial factors that influence the reflection probability of a condensate containing a dark soliton, in particular, the orientation of the dark soliton (θ), the widths of the potential wells and barriers (d), and the expansion of the condensate cloud. By comparing the results of potential wells and potential barriers, we find that the orientation of a dark soliton in the condensate does affect the quantum reflection of the condensate in a non-trivial way. The dependence of the reflection probabilities on the orientation of the dark soliton for both potential wells and barriers can be unifiedly described by a function in the form of $R(\theta) \sim \cos[\lambda(\theta - \pi/2)]$, where λ is a parameter related to d. For potential barriers, $\lambda = 2$ is a good approximation to fit the R_s–θ curves. However, the dependence of λ on d is quite complicated for potential wells, where λ may choose its value in a wide range from negative to positive according to d. The dependence of the reflection probability on the width of potential wells or barriers obeys completely different rules. For potential wells, R_s shows a damped oscillation to a stable value until d is larger than the length of the dark soliton (size of the condensate cloud). For potential barriers, R_s increases monotonically until reaching its asymptotic value when d is larger than the decay length of the barrier which is determined by the decay constant $\beta \simeq \sqrt{2m(V_0 - E)/\hbar^2}$ ($V_0 > E$). R_s is sensitive to θ for a potential well within the size of the condensate cloud, while R_s shows differences for varying θ for a potential barrier when $d > x_0$. While the reflection probability for a potential well is much smaller than that for a potential barrier, the sensitivity to θ can be greatly improved. The sensitivity of reflection probability on the orientation of the soliton for potential wells may permit experiments to detect the existence of a dark soliton and probe the possible structure. These results are useful for better understanding of the underlying mechanism of a BEC with a dark soliton reflected from a step potential and the physics behind the experimental observations of BECs with solitons reflected from more complex semiconductor-surface and nanostructure potentials. The dark-bright solitons in multi-component BECs have novel dynamical properties due to the novel nonlinear structures. It has been shown that the dark soliton can modify the spectral shape and the splitting of the bright soliton.[50] The spin-orbit coupled strength affects interaction types (attractive or repulsive) between the two dark-bright solitons.[51] It is interesting to study the quantum reflection properties of this kind of symbiotic solitons.

Acknowledgment

We thank Xue Yang and Wen-Kai Bai for helpful discussions.

References

[1] Friedrich H and Trost J 2004 *Phys. Rep.* **397** 359
[2] Landau L D, Landau L D and Landau L D 1992 *Lehrbuch der Theoretischen Physik III. Quantenmechanik* (Europa Lehrmittel Verlag)
[3] Landragin A, Courtois J Y, Labeyrie G, Vansteenkiste N, Westbrook C I and Aspect A 1996 *Phys. Rev. Lett* **77** 1464
[4] Segev B, Côté R and Raizen M G 1997 *Phys. Rev. A* **56** R3350
[5] Côté R, Segev B and Raizen M G 1998 *Phys. Rev. A* **58** 3999
[6] Pasquini T A, Saba M, Jo G B, Shin Y, Ketterle W, Pritchard D E, Savas T A and Mulders N 2006 *Phys. Rev. Lett* **97** 093201
[7] Dufour G, Guérout R, Lambrecht A, Nesvizhevsky V V, Reynaud S and Voronin A Yu 2013 *Phys. Rev. A* **87** 022506
[8] Zhao B S, Schewe H C, Meijer G and Schöllkopf W 2010 *Phys. Rev. A* **105** 133203
[9] Shimizu F 2001 *Phys. Rev. Lett.* **86** 987
[10] Scott R G, Martin A M, Fromhold T M and Sheard F W 2005 *Phys. Rev. Lett.* **95** 073201
[11] Pasquini T A, Shin Y, Sanner C, Saba M, Schirotzek A, Pritchard D E and Ketterle W 2004 *Phys. Rev. Lett.* **93** 223201
[12] Silvestre M, Cysne Tarik P, Szilard D, Pinheiro F A and Farina C 2019 *Phys. Rev. A* **100** 033605
[13] Judd T E, Scott R G, Martin A M, Kaczmarek B and Fromhold T M 2011 *New J. Phys.* **13** 083020
[14] Cornish S L, Parker N G, Martin A M, Judd T E, Scott R G, Fromhold T M and Adams C S 2009 *Physica D* **238** 1299
[15] Dodd, Roger K, Eilbeck, Chris J, John D, Morris and Hedley C 1982 *Solitons and Nonlinear Wave Equations* (New York: Academic Press)

[16] Hirota and Ryogo 1973 *J. Math. Phys.* **14** 810

[17] Kuznetsov E A, Rubenchik A M and Zakharov V E 1987 *Physics Reports* **142** 103

[18] Lonngren K E 2000 *Plasma Phys.* **25** 943

[19] Tang D Y, Zhang H, Zhao L M and Wu X 2008 *Phys. Rev. Lett.* **101** 153904

[20] Gibbon J D, Caudrey P J, Bullough R K and Eilbeck J C 1973 *Lettere Al Nuovo Cimento* **8** 775

[21] Zabusky N J 1968 *Phys. Rev.* **168** 124

[22] Newell A C 1980 *The Inverse Scattering Transform* (Berlin: Springer)

[23] Proukakis N P, Parker N G, Frantzeskakis D J and Adams C S 2004 *J. Opt. B* **6** S380

[24] Wu M Z, Kalinikos B A and Patton C E 2004 *Phys. Rev. Lett.* **93** 157207

[25] Sakaguchi H and Malomed B A 2016 *New J. Phys.* **18** 025020

[26] Burger S, Bongs K, Dettmer S, Ertmer W, Sengstock K, Sanpera A, Shlyapnikov G V and Lewenstein M 1999 *Phys. Rev. Lett.* **83** 5198

[27] Denschlag J, Simsarian J E, Feder D L, Clark Charles W, Collins L A, Cubizolles J, Deng L, Hagley E W, Helmerson K and Reinhardt W P 2000 *Science* **287** 97

[28] Denschlag J, Simsarian J E, Feder D L, Clark C W, Collins L A, Cubizolles J, Deng L, Hagley E W, Helmerson K and Reinhardt W P 1999 *Generating Solitons by Phase Engineering of a Bose–Einstein Condensate* (Laser Cooling: Bose–Einstein Condensation and Atom Laser–Proceedings of CCAST (World Laboratory Workshop)

[29] Stellmer S, Becker C, Soltan-Panahi P, Richter E-M, Dörscher S, Baumert M, Kronjäger J, Bongs K and Sengstock K 2008 *Phys. Rev. Lett.* **101** 120406

[30] Anderson B P, Haljan P C, Regal C A, Feder D L, Collins L A, Clark C W, Cornell E A 2001 *Phys. Rev. Lett.* **86** 2926

[31] Engels P and Atherton C 2007 *Phys. Rev. Lett.* **99** 160405

[32] Chang J J, Engels P and Hoefer M A 2008 *Phys. Rev. Lett.* **101** 170404

[33] Jo G B, Choi J H, Christensen C A, Pasquini T A, Lee Y R, Ketterle W and Pritchard D E 2007 *Phys. Rev. Lett.* **98** 180401

[34] Weller A, Ronzheimer J P, Gross C, Esteve J, Oberthaler M K, Frantzeskakis D J, Theocharis G and Kevrekidis P G 2008 *Phys. Rev. Lett.* **101** 130401

[35] Jurisch A and Rost J M 2010 *Phys. Rev. A* **81** 043610

[36] Scott R G, Hutchinson D A W and Gardiner C W 2006 *Phys. Rev. A* **74** 053605

[37] Martin A D, Adams C S and Gardiner S A 2007 *Phys. Rev. Lett.* **98** 020402

[38] Martin A D, Adams C S and Gardiner S A 2008 *Phys. Rev. A* **77** 013620

[39] Lee C and Brand J 2005 *Europhys. Lett.* **73** 321

[40] Xu T F, Zhang Y F, Xu L C and Li Z D 2017 *Chin. Phys. B* **26** 100304

[41] Xu Y, Zhang Y and Wu B 2013 *Phys. Rev. A* **87** 013614

[42] M Liu, L She, H W Xiong and M S Zhan 2006 *Phys. Rev. A* **74** 043619

[43] Martin A M, Scott R G and Fromhold T M 2007 *Phys. Rev. A* **75** 065602

[44] Cheng Q L, Bai W K, Zhang Y Z, Xiong B and Yang T 2019 *Laser Phys.* **29** 015501

[45] Sciacca M, Barenghi C F and Parker N G 2017 *Phys. Rev. A* **95** 013628

[46] Gaunt A L, Schmidutz T F, Gotlibovych I, Smith R P and Hadzibabic Z 2013 *Phys. Rev. Lett.* **110** 200406

[47] Meyrath T P, Schreck F, Hanssen J L, Chuu C S and Raizen M G 2005 *Phys. Rev. A* **71** 041604(R)

[48] Xiong B, Yang T and Benedict K A 2013 *Phys. Rev. A* **88** 043602

[49] Yang T, Xiong B and Benedict K A 2013 *Phys. Rev. A* **87** 023603

[50] Liu Z, Jia W G, Wang H Y, Wang Y, Neimule M K and Zhang J P 2020 *Chin. Phys. B* **29** 064212

[51] Xu T F, Li W L, Li Z D and Zhang C 2018 *Chaos, Solitons & Fractals* **111** 62